THE ASTROPHYSICAL JOURNAL, 427:L21–L24, 1994 May 20

HUBBLE SPACE TELESCOPE FINE GUIDANCE SENSOR INTERFEROMETRIC OBSERVATIONS OF THE CORE OF 30 DORADUS

M. G. LATTANZI,[1,2,3] J. L. HERSHEY,[4] R. BURG,[5,1] L. G. TAFF,[1] S. T. HOLFELTZ,[1] B. BUCCIARELLI,[1,3]
I. N. EVANS,[1] R. GILMOZZI,[1,2] J. PRINGLE,[6] AND N. R. WALBORN[1]
Received 1994 January 14; accepted 1994 March 2

ABSTRACT

We present the results of the first high angular resolution observations taken with a Fine Guidance Sensor (FGS) aboard the *Hubble Space Telescope* (*HST*) of a star cluster embedded in very bright background. The strong and complex background around the R136 cluster in the 30 Dor nebula does not prevent the FGS from achieving performance close to its angular resolution limit of approximately 0.″015 per axis with reliable photometry. These FGS observations establish that the central object in R136a is a triple star with the third component $\Delta V = 1.1$ mag fainter than the primary star a1 $\sim 0.''08$ away. We estimate from the grid of models of Maeder (1990) that the present mass of a1 is between 30 and 80 solar masses, with the main-sequence progenitor between 60 and 120 solar masses.

Subject headings: Magellanic Clouds — stars: early-type — stars: luminosity function, mass function — stars: Wolf-Rayet — techniques: interferometric

1. INTRODUCTION

The establishment of an upper mass limit for individual stars remains an open question of great importance in astronomy. Its resolution will influence the studies of the evolution of stars, H II regions, and galaxies. Observations of the giant H II region 30 Doradus have provided some of the best candidates for the most massive stars. In this *Letter*, we report on high angular resolution observations of the bright core of the massive star cluster R136 within 30 Doradus, R136a, which had for many years been unresolved and whose structure and photometry are still not fully explored.

The measurements were performed using the TRANSfer Mode of the Fine Guidance Sensor 3 (FGS3) as part of the FGS Cycle 3 Calibration program. We have detected 10 sources within 1″, with a resolution of approximately 0.″015 per axis. Accurate astrometry (to $\sim 0.''010$ or better in separation and $\sim 1°$ in position angle) and new V-band photometry (to 0.1 mag, internal error) are provided for most of these components. The mass of the brightest component of R136a, based solely on the FGS photometry of the resolved stars, is estimated.

2. TECHNIQUE AND MEASUREMENTS

Bradley et al. (1991) and Taff (1990, 1991) provide a detailed description of the FGS optical system, operating modes, and calibration principles. The FGS measurements consist of 10 identical position angle, consecutive scans, each 2.″1 long with a step size of 0.″0006, through R136a. The Transfer Function (TF) refers to the fringe visibility pattern produced by the Koester's prism-based interferometers inside the FGS when the $5'' \times 5''$ instantaneous field-of-view (FOV) is scanned across an object. A polarizing beam-splitter before the prisms provides sensitivity in two orthogonal directions, referred to as the X and Y directions in detector space. The fringe is detected by two pairs of photomultipliers (PMTs), one pair per axis. We can regard the $X(Y)$ scan as driving a slit of the size of the resolution limit in $X(Y)$ and 5″ wide in the $Y(X)$ direction along the scan path. The TFs of the reference single star used as a template in this study are shown in Figure 1. Another object appearing anywhere in the rectangular slit has the same projected $X(Y)$ coordinate, within the resolution limit, as that of the primary target. The resulting fringe will have an amplitude that is the sum of the two individual fringe amplitudes.

The actual geometry of the scans is shown in Figure 2. The star field is that of the high-resolution FOC F/288 image discussed by Weigelt et al. (1991, page L22). The orientation of the detector axes as projected onto the plane of the sky is also shown. "Actual Scan" defines the path of the center of the FGS FOV as it moved across the star field, while "Center of Scan" identifies the location to which the center of the FOV was commanded at the end of the acquisition procedure. A pointing bias of about 0.″5 (subsequently removed from the acquisition procedure) is evident. However, given the large FOV, this bias did not prevent the observation from being successful, although in consequence the X, but not the Y, scan fell short of reaching stars a3 and a6. The scan direction makes a 45° angle to the X and Y axes (about 1.″5 each in length).

The PMT integration time was 0.025 s. To increase the signal-to-noise ratio (S/N) 10 consecutive scans were taken and added together for a total exposure time of 10.3 minutes. Each individual scan has a S/N of about 3. Co-adding the scans together increases the S/N to ~ 11, consistent with the expected improvement of $\sqrt{10}$.

The spherical aberration of the primary combined with known FGS misalignments causes a reduction of the visibility function and adds spurious structures to the TF. Optimal sensitivity for detection in a complex region is obtained by using the PUPIL position in the filter wheel. This introduces a field stop into the beam that eliminates most of the aberration to the wave front by reducing by $\frac{1}{3}$ the effective mirror diam-

[1] Space Telescope Science Institute, 3700 San Martin Drive, Baltimore, MD 21218.
[2] Affiliated with the Space Sciences Department, ESA.
[3] On leave from Osservatorio di Torino.
[4] Astronomy Programs, Computer Sciences Corporation at Space Telescope Science Institute.
[5] Department of Physics and Astronomy, the Johns Hopkins University.
[6] Institute of Astronomy, Madingley Road, Cambridge, CB3 0HA, England.

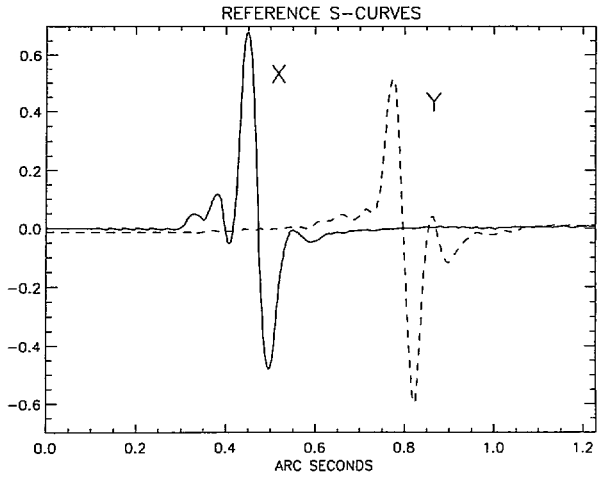

FIG. 1.—Normalized Transfer Functions (TFs) of the reference single star Upgren 69 taken through the PUPIL filter. The thick curve labeled X refers to the *X*-axis TF; the dashed curve represents the *Y*-axis TF. Note that the relative peak-to-peak amplitude is ~1.1 for both TFs.

eter. Although angular resolution is formally reduced by $\frac{1}{3}$, we observed R136a with the PUPIL.

An accurate photometric calibration of the PUPIL filter has not been carried out by the observatory. A careful comparison of the throughput of the FGS with the PUPIL and with the F583W (clear) filter shows that the bandpasses are quite similar (Abramowicz-Reed 1994), with the blue cutoff at ~4600 Å defined by the FGS relay optics and the red cutoff at ~7000 Å defined by the S20 cathode. We have, therefore, adopted for use with the PUPIL the effective wavelength of 5830 Å, bandpass of 2340 Å, and the carefully calibrated transformation to Johnson-*V* for the F583W filter determined by Bucciarelli et al. (1994). This calibration shows that, for hot stars, the color correction would amount to less than 0.05 mag.

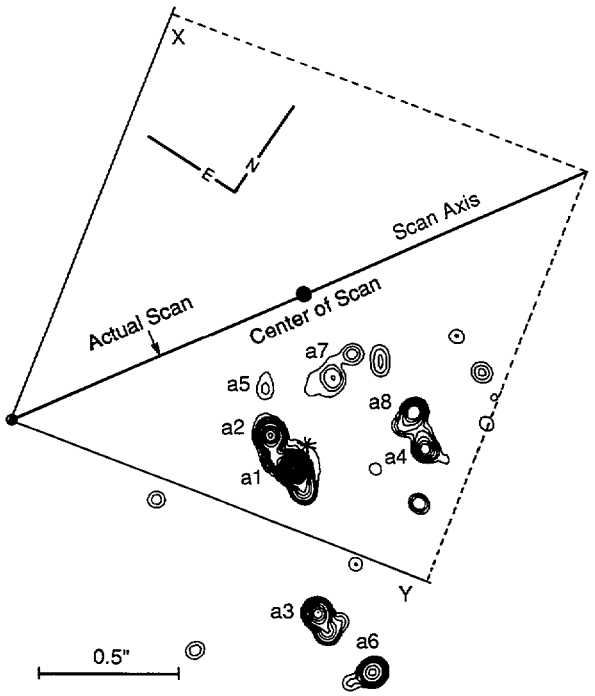

FIG. 2.—Overlay of the geometry of the FGS scan with the F/288 FOC image of Weigelt et al. (1991). The figure shows the innermost 1".7 × 1".7 of the 30 Dor core. The location of the new component a1B is denoted by an asterisk(*).

Although the algorithms described in Hershey (1992), Lattanzi et al. (1992), and Bernacca et al. (1993) for measuring double stars must be modified to deal with the complexity of R136a, the basic technique remains unaltered. Simply, the measurement of separations and magnitude differences of multiple component objects is performed, as for double stars, by measuring the departures of the corresponding TFs from the template TFs of a reference single star. The *X* and *Y* template TFs shown in Figure 1 were taken with the PUPIL on our reference single star Upgren 69 in NGC 188 (see Bernacca et al. 1993 and references therein) and are closest, both in time and in detector space, to the observations of R136a. The procedure described in Lattanzi et al. (1992) has been generalized as follows. A set of equal brightness and equally spaced single-star TFs are "placed" on a scan. The location of the first component is shifted stepwise while the others are kept fixed and a synthetic TF model is calculated at every step. The least-squares minimum in the residual curve TF(model)–TF(observed) yields the best location for the current star. With the star fixed at this location, a new minimum is searched for by varying the intensity of this star relative to the others. Relative intensity and position fully characterize the contribution of this component to the model scan. After going through all the components initially placed on a scan, the procedure is iterated to make sure that a global minimum is found. Final inspection of the residuals reveals if more components are necessary at particular locations along the scans, in which case, the program is restarted from the beginning. Twenty-four stars were used in this investigation. Figures 3*a* and 3*b* show the results for the *X* and *Y* scans, respectively. The thick curves represent the observed TFs, and the dashed lines superimposed are the residual curves. The locations and relative amplitudes, proportional to the relative brightnesses, of the "spikes" appearing on the abscissas represent the solutions of our adjustments. The dashed curves shown in the bottom part of Figures 3*a* and 3*b* represent the result of applying Hershey's (1992) deconvolution technique to the *observed* TFs. There is quite good agreement between this independent method and the other solutions. As expected, Hershey's deconvolved TFs generally overlay the locations and the relative amplitudes of the set of point source positions deduced from the synthetic TF method. At this stage, local variations must be attributed to the limitations of the present implementation of the synthetic TF method, as the deconvolved TFs contain all the information of the co-added scans.

3. RESULTS AND THE MASS OF R136a1 REVISITED

The unambiguous identification of components a1 and a2 from our solution is simple, since they are the closest, most luminous pair of objects in the field. The finite resolving power of the instrument, and the crowded field, make the firm identifications of the remaining sources on the sky impossible (see § 2). Even two independent directions will not solve the problem, although for a given resolution limit there is a minimum non-redundant set that will. Alternatively, we can use images of comparable resolution to help establish the identifications. Thanks to the extensive observational campaign in this field with the FOC and the PC during the last three years, we now have images that can be used for this purpose. The identifications shown in Figures 3*a* and 3*b* combine the results of pro-

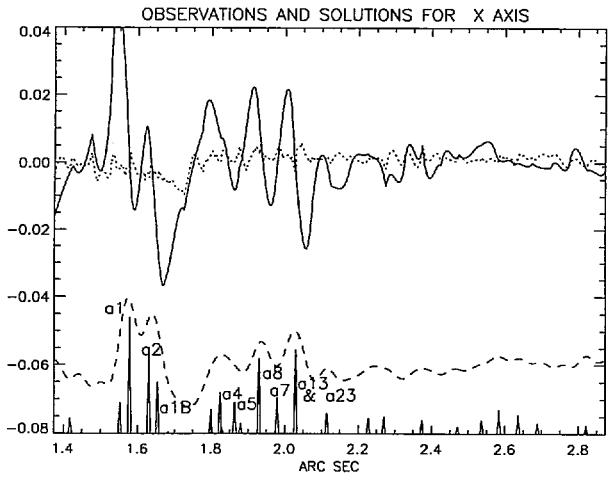

FIG. 3a

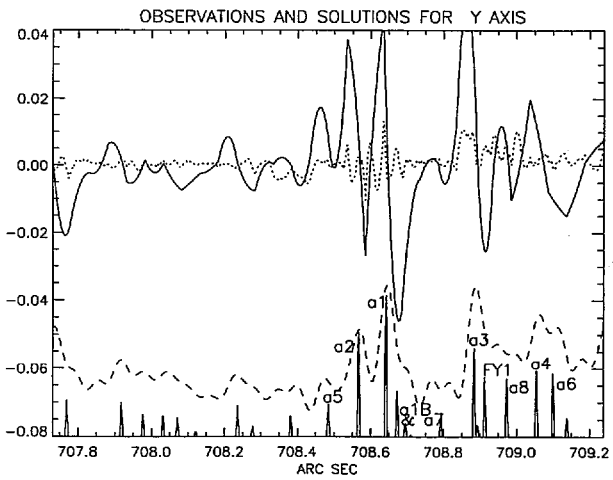

FIG. 3b

FIG. 3.—The results of interpreting the 30 Dor signal on the X (a) and Y (*b*) axes. Thick curves are the normalized observed TFs, dotted lines are the residual curves, and dashed curves are the profiles generated from the deconvolution of the TFs. The low peak-to-peak amplitude of these TFs, compared to those of Fig. 1, is due to the very high background which depresses the fringe visibility of the stellar sources. The position and relative amplitude of the spikes on the abscissa represent the individual stellar components from our adjustments. The amplitude of the spikes is proportional to the relative brightness of the components. Only the sharpest features are identified (see text).

jecting the FOC f/288 image discussed in Weigelt et al. (1991) and the F368M PC image of Campbell et al. (1992, plate 115) onto the FGS X and Y axes. For this *Letter*, we have limited the identifications to the "classical" eight objects of Weigelt & Baier (1985) and to new components which appear as close companions of some of them. This is justified since our simulations show that, in excess of the 99.7% confidence level, no spike with a relative amplitude above 0.015 can be spurious.

Table 1 lists separations (ρ), position angles (PAs) (J2000 equinox), and magnitude differences (ΔV Johnson per axis and average) with respect to star a1, according to the identifications given in Figures 3*a* and 3*b*. The ρ's and the PAs have been derived from the projected separations reported in detector space in Table 1 (detector space is a double, north-south and east-west, reflection of the FGS axes shown in Fig. 2). For components a3 and a6 we have only the Y scan, as mentioned earlier in § 2. The location on the sky of component a1B is marked with an asterisk (*) in Figure 2. This new component of the a1-a2 system is about 1.1 mag fainter than a1 and 0".08 away from it. On the Y scan, a7 is partially aligned with the a1-a2 system (as seen on the FOC and PC images). According to the X scan magnitudes, a7 is 0.4 mag fainter than a1B. This explains the less satisfactory quality of the fit near the spikes identified as "a1B and a7" on the Y scan (Fig. 3*b*) when compared to the residuals near the X-scan spike of a1B, but the magnitude difference is still consistent between the two axes. A third component is also in Campbell et al. (1992; see their star number 9 in Table 2) but not in Weigelt et al. (1991) or in the most recent ground-based speckle work at $\lambda \sim 7000$ Å by Pehlemann, Hoffman, & Weigelt (1992). Component a9 given in Campbell et al. (1992) has an F555W magnitude comparable to that of stars a1 and a2, while we see a somewhat fainter star, and the PA in Campbell et al. (1992) is significantly different from that of component a1B reported here. The smallest projected separation resolved here is ~0".025 between a1B and a2, which is consistent with the 0".015 resolution limit established through Monte Carlo simulations (Lattanzi et al. 1992).

TABLE 1

THE STELLAR CONTENT OF R136a

	SEPARATIONS				MAGNITUDES		
IDENTIFICATION	Δx	Δy	ρ	PA	ΔV_x	ΔV_y	$\langle \Delta V \rangle$
1	...	...	...	...	...	...	...
2	0".05	−0".08	0".09	66°	0.4	0.3	0.4
1B	0.08	0.03	0.08	349	0.9	1.2	1.1
3	...	0.24	...	...	...	0.5	0.5
FY1	...	0.27	...	...	...	0.9	0.9
4	0.25	0.41	0.48	312	1.1	0.8	1.0
5	0.29	−0.16	0.33	40	1.4	1.6	1.5
6	...	0.46	...	...	...	0.9	0.9
7	0.40	0.03	0.40	7	1.3	1.2	1.3
8	0.35	0.33	0.48	328	0.5	1.0	0.8

Campbell et al. (1992) list a10 and a11 as close companions of a3 and a6, respectively. FY1 is our candidate for a10, although the FGS photometry is ~0.7 mag brighter. The projection of the field is particularly crowded in that portion of the Y scan, and in the absence of an X scan (which would yield a much clearer signal in this case) we expect a larger error in our photometry. Therefore, FY1 is most likely Campbell et al's object a10. As for a11, we see a component in our Y-axis solution at about 709".138 (Fig. 3*b*), about 0".040 away from a6, consistent with the total separation given in Campbell et al. (1992) (~0".070). However, a11 is 0.5 mag brighter than a6 according to the PC photometry, and our candidate for a11 is 1.3 mag fainter than a6, which is fainter than the mag limit of interest here. Components a4 and a8 are clearly resolved with a separation of 0".13. Star a8 has the largest discrepancy between ΔV_X and ΔV_Y with ΔV_Y probably with a larger error as the X-scan solution shows better agreement between the synthetic method and the deconvolved TF. Finally, the sharp spike at 2".029 seen on the X-axis is identified as "a13 and a23." The FOC and PC images show that it is an almost perfect chance alignment (a12 of Campbell et al. 1992 is also included) of stars of comparable magnitude as discussed in § 2. In Campbell et al. (1992) a13 and a23 are about the same F555W magnitude, and a12 is ~0.5 mag fainter. In the case of perfect alignment, we can predict from the F555W PC data and the discussion in

§ 2 that the three stars together would appear only 0.2 mag fainter than a1. The value from the X-axis solution for "a13 and a23" is 0.36 mag, giving us added confidence in our technique.

Following the discussions of Walborn (1984, 1986), we adopt the values of $V_0 - M_V = 18.6$ (Panagia et al. 1991), $A_V = 1.2$ (Savage et al. 1983), and $V(a) = 10.77$ for the integrated magnitude of R136a (Schmidt-Kaler & Feitzinger 1981). The relative magnitudes in Table 1, although generally consistent with previous work, do show significant differences. Thus, they provide new material with which to estimate the mass of R136a1. These numbers imply $M_V(a) = -9$ for R136a. Recently, De Marchi et al. (1993) have used $A_V = 1.39$ and $V \sim 11$. These values yield almost exactly the same number for $M_V(a)$. From the photometry in Table 1 we derive $V(a1) - V(a) = 1.75$, implying $M_V(a1) = -7.25$. Campbell et al. (1992) have established that component a1 is a W-R star. Moffat, Seggewiss, & Shara (1985; see also Walborn 1973) classify the R136a complex as being no later than type WN6. A lower limit for the luminosity of a1 is set by adopting the bolometric correction (BC) for type WN6, BC $= -3.6$ (Schmidt-Kaler 1982). We obtain $M_{bol}(a1) = -10.85$ and $\log (L/L_\odot) = 6.24$ ($\log T_e = 4.59$). By assuming spectral type WN3, the upper limit for the luminosity is $M_{bol}(a1) = -11.69$ (BC $= -4.4$) and $\log (L/L_\odot) = 6.58$ ($\log T_e = 4.70$).

Using Maeder's models (1990) for solar metallicity, these luminosities imply a present-day mass between 40 and 70 $M_\odot$, main-sequence progenitor mass between 60 and 120 $M_\odot$, and age between 3.6 and 2.6 Myr. Since the metallicity of the LMC is lower than the Galaxy's, we also adopt a metallicity of 0.25 $Z_\odot$ as in De Marchi et al. (1993). In this case, Maeder's models predict a present-day mass between 30 and 80 $M_\odot$, main-sequence progenitor mass between 60 and 120 $M_\odot$, and age between 4.4 and 2.8 Myr. These values are the lowest for the direct mass determination of a1 and are consistent with the limits derived from isochrone fitting of UV color-magnitude diagrams (De Marchi et al. 1993). We note that ground-based spectroscopy favors the WN6 classification for a1 and therefore the lower limit on the mass. Finally, the potential exists that a1 could reveal itself as a multiple star below the FGS limit of 1000 AU at the distance of the LMC.

4. CONCLUSIONS

In this *Letter* we have presented the first FGS interferometric observation of a crowded field embedded in high background. This observation resulted in a new mapping of the R136a cluster with 0.″015 resolution per axis and V photometry to 0.1 magnitude. We provide evidence for a third component, a1B, within the a1-a2 system with a separation of 0.″08, or a distance of approximately 4000 AU from a1. Finally, our photometry indicates that the range for the present mass of the W-R star R136a1 is between 30 and 80 $M_\odot$, with a main-sequence progenitor between 60 and 120 $M_\odot$. We stress that these are global upper limits, since a1 could still be a multiple system with separations less than 1000 AU.

Based on observations with the NASA/ESA *Hubble Space Telescope* (*HST*), obtained at the Space Telescope Science Institute, which is operated by the Association of Universities for Research in Astronomy, Inc., under NASA contract NAS 5-26555. Supported in part by NASA grants NAGW-2597 and CW-0016-92. R. B. is partially supported by NASA grant NAGW-2509. I. N. E. is supported partially by NASA grant NAG 5-1630. We are grateful to P. Bely, H. Burg, and F. Paresce for very useful discussions and comments all throughout this work. We wish to thank F. Macchetto and P. Stockman for their careful reviews during the preparation of the calibration observations. Finally, we wish to thank the members of the *HST* Astrometry Team (led by W. Jefferys) for stimulating discussions during their regular meetings.

REFERENCES

Abramowicz-Reed, L. (HDOS) 1994, private communication
Bernacca, P. L., et al. 1993, A&A, 278, L47
Bradley, A., Abramowicz-Reed, L., Story, D., Benedict, G., & Jefferys, W. 1991, PASP, 103, 317
Bucciarelli, B., Holfeltz, S. T., Lattanzi, M. G., Taff, L. G., & Vener-Saavedra, P. C. 1994, PASP, in press
Campbell, B., et al. 1992, AJ, 104, 1721
De Marchi, G., Nota, A., Leitherer, C., Ragazzoni, R., & Barbieri, C. 1993, ApJ, 419, 658
Hershey, J. L. 1992, PASP, 104, 592
Lattanzi, M. G., Bucciarelli, B., Holfeltz, S. T., & Taff, L. G. 1992, IAU Colloq. 105, Complementary Approaches to Double and Multiple Star Research, ed. H. A. McAlister & W. I. Hartkopf (ASP Conf. Ser., 32), 377
Maeder, A. 1990, A&AS, 84, 139
Moffat, A. F. J., Seggewiss, W., & Shara, M. M. 1985, ApJ, 295, 109
Panagia, N., Gilmozzi, R., Macchetto, F., Adorf, H.-M., & Kirshner, R. P. 1991, ApJ, 380, L23
Pehlemann, E., Hoffman, K.-H., & Weigelt, G. 1992, A&A, 256, 701
Savage, B. D., Fitzpatrick, E. L., Cassinelli, J. P., & Ebbetts, D. C. 1983, ApJ, 273, 597
Schmidt-Kaler, T. 1982, in Landolt-Börnstein, Numerical Data and Functional Relationships in Science and Technology, Vol. 2B, ed. K. Schaifers & H. H. Voigt (Berlin: Springer), 452
Schmidt-Kaler, T., & Feitzinger, J. V. 1981, ESO Workshop on the Most Massive Stars, ed. S. D'Orico, D. Baade, & K. Kjar (Garching: ESO), 105
Taff, L. G. 1990, ApJ, 365, 407
———. 1991, Adv. Space Res., 11, 97
Walborn, N. R. 1973, ApJ, 179, 517
———. 1984, IAU Symp. 108, Structure and Evolution of the Magellanic Clouds, ed. S. Van der Bergh & K. S. de Boer (Dordrecht: Reidel), 243
———. 1986, IAU Symp. 116, Luminous Stars and Associations in Galaxies, ed. C. W. H. de Loore, A. J. Willis, & P. Laskarides (Dordrecht: Reidel), 185
Weigelt, G., & Baier, G. 1985, A&A, 150, L18
Weigelt, G., et al. 1991, ApJ, 378, L21